Dalton Transactions

ROYAL SOCIETY OF CHEMISTRY

PAPER

View Article Online
View Journal | View Issue



Check for updates

Cite this: *Dalton Trans.*, 2023, **52**, 2712

# Factors controlling the structure of alkylzinc amidinates: on the role of *N*-substituents†

Michał Terlecki, [a] Iwona Justyniak, [b] Michał K. Leszczyński, [a,b] Piotr Bernatowicz [b] and Janusz Lewiński *[a,b]

Received 18th November 2022,
Accepted 3rd February 2023

DOI: 10.1039/d2dt03722j

rsc.li/dalton

Despite various applications of alkylzinc complexes supported by *N*,*N*-bidentate ligands in chemistry and materials science, the corresponding organozinc amidinates still represent an insufficiently explored area. To gain a more in-depth understanding of factors controlling the structure and stability of alkylzinc amidinates, we selected benzamidinate and *N*,*N*′-diphenylformamidinate ligands as model *N*,*N*′-unsubstituted and *N*,*N*′-diaryl substituted ligands, respectively, to systematically modify the secondary coordination sphere of the Zn center. A series of new alkylzinc amidinates has been synthesized and their molecular structures identified in both the solid state (single-crystal X-ray crystallography) and solution (NMR and FTIR spectroscopy). The results indicate that $[RZnL]_x$-type amidinate moieties are essentially unstable and tend to undergo Schlenk equilibria-mediated ligand scrambling leading to more thermodynamically stable non-stoichiometric $[R_2Zn_3L_4]$- and $[R_3Zn_4L_5]$-type complexes. This process is significantly influenced by the secondary coordination sphere noncovalent interactions as well as the steric hindrance provided by both zinc-bounded alkyl groups and the *N*-substituents.

## Introduction

Heteroleptic alkylzinc compounds are of longstanding interest due to their important role in various stoichiometric and catalytic chemical processes[1–7] and more recently as efficient predesign precursors of modern functional materials.[8–11] However, the characterization of organozinc reactants and intermediate states is often challenging as they commonly exhibit complicated behavior in solutions involving multiple equilibria between various aggregated forms and non-stoichiometric species arising from Schlenk equilibria.[2,12–15] The nature and reactivity of heteroleptic alkylzincs are often not only determined by the primary coordination sphere (*i.e.*, the array of the direct metal–ligands interactions) but they can be strongly influenced by the secondary coordination sphere interactions of the metal environment,[16,17] which includes organic skeletons of supporting ligands or external functionalities attached to the internal scaffolds that not only provide a specific steric environment but may participate in an array of noncovalent interactions and be very effective in the construction of supramolecular assemblies.[18–21] Hence, many of the important transformations involving alkylzinc compounds are still not well understood, such as, among others, the fascinating autocatalytic Soai reaction,[5,7] and the oxygenation of organozincs, which mechanism has been under debate for over 160 years.[22,23] In this view, a more in-depth understanding of the multifaceted chemistry of alkylzinc species is crucial for the development of new, more efficient reaction systems.

Among various supporting ligands used for the stabilization of heteroleptic organozinc complexes amidinates are particularly interesting due to a prominent tunability of steric and electronic requirements by systematic variations of the substituents at the carbon and nitrogen atoms.[24–26] These ligands exhibit a vast array of coordination modes, including $\mu_2$-bridging, $\kappa^2$-chelating, as well as more complex $\mu_3$-bridging and mixed bridging–chelating $\mu_2$-$\kappa^2$:$\kappa^1$ (Fig. 1b), which originates in a specific parallel orientation of the N donor electron pairs in the NCN anchoring groups that can be tuned by for example sterically demanding substituents or strains in macrocycle organic backbones (Fig. 1a).[24,25,27] Furthermore, amidinate ligands introduce N-bonded hydrogen atoms or organic groups like aromatic rings or bulky alkyls to the proximity of the metal center that can interfere with its primary coordination sphere either by steric hindrances blocking the access to the metal ion[28] or noncovalent interactions providing specific structural stabilization.[29] A particularly interesting example of the influence of *N*-substituents on the stabilization of molecular structure of alkylzinc complexes concerns

[a]*Faculty of Chemistry, Warsaw University of Technology, Noakowskiego 3, 00-664 Warsaw, Poland. E-mail: lewin@ch.pw.edu.pl*
[b]*Institute of Physical Chemistry, Polish Academy of Sciences, Kasprzaka 44/52, 01-224 Warsaw, Poland*

†Electronic supplementary information (ESI) available. CCDC 2220050–2220053. For ESI and crystallographic data in CIF or other electronic format see DOI: https://doi.org/10.1039/d2dt03722j

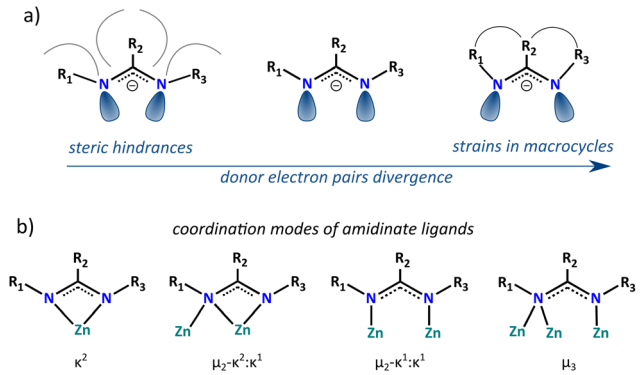


**Fig. 1** (a) Tunable spatial orientation of the donor electron pairs in NCN anchoring groups; (b) coordination modes of amidinate ligands in zinc coordination systems.

*N*,*N*′-diaryl amidinate ligands. Introduction of sterically demanding substituents to the *ortho* position of N-bonded aromatic rings results in the decrease of nuclearity of the respective alkylzinc systems from a trinuclear $[Et_2Zn_3(dipf)_4]$ in the case of *ortho*-unsubstituted *N*,*N*′-diphenylformamidinate (dipf) ligands to a dinuclear aggregate $[Et_2Zn_2L_2{\cdot}THF]$ for the 2,6-dimethyl or 2-isopropyl analogs[28] and a monomeric complex $[MeZn\{^tBuC(NDipp)_2\}]$ comprising 2,6-diisopropylphenyl (Dipp) *N*-substituents.[29] Furthermore, aromatic rings in the secondary coordination sphere are prone to participate in specific CH–π, π–π, or ion–π interactions, which may also affect the stabilization of the coordination system. For instance, ligands in $[MeZn\{^tBuC(NDipp)_2\}]$ adopt an unusual $\kappa^1{:}\eta^3$ coordination mode involving efficient stabilization of the low coordinated zinc center *via* a Zn–π interaction (Fig. 2a).[29] Theoretical calculations revealed that this type of coordination is slightly preferred, by only 1.5 kcal $mol^{-1}$, over the common chelating $\kappa^2$ mode, which shows that noncovalent interactions involving aromatic π systems may effectively compete with the formation of donor–acceptor bonds (this type of structural diversity has been observed for some other heteroleptic zinc alkyls[30–32]).

In turn, *N*,*N*′-unsubstituted amidinates involving NH units are an interesting group of ligands that can participate in the formation of intra- and intermolecular hydrogen bonds in the proximity of the coordination center. Strikingly, the chemistry of alkylzinc complexes supported by this type of ligands is highly unexplored, and, as far as we know, a series of macrocyclic trimeric group 13 benzamidinates, $[Me_2M(bza)]_3$ (M = Al, Ga, In; bza–H = benzamidine) was until now the only example of structurally characterized main group organometallics incorporating *N*,*N*′-unsubstituted amidinates.[33] Very recently, we used *in situ* generated alkylzinc derivatives of benzamidine as efficient precursors of zinc–oxido clusters[21] and zinc oxide nanostructures.[11] In these studies, we found that the NH units of the benzamidinate ligands play important role in the stabilization of ZnO nanocrystals' surface providing H-donor sites

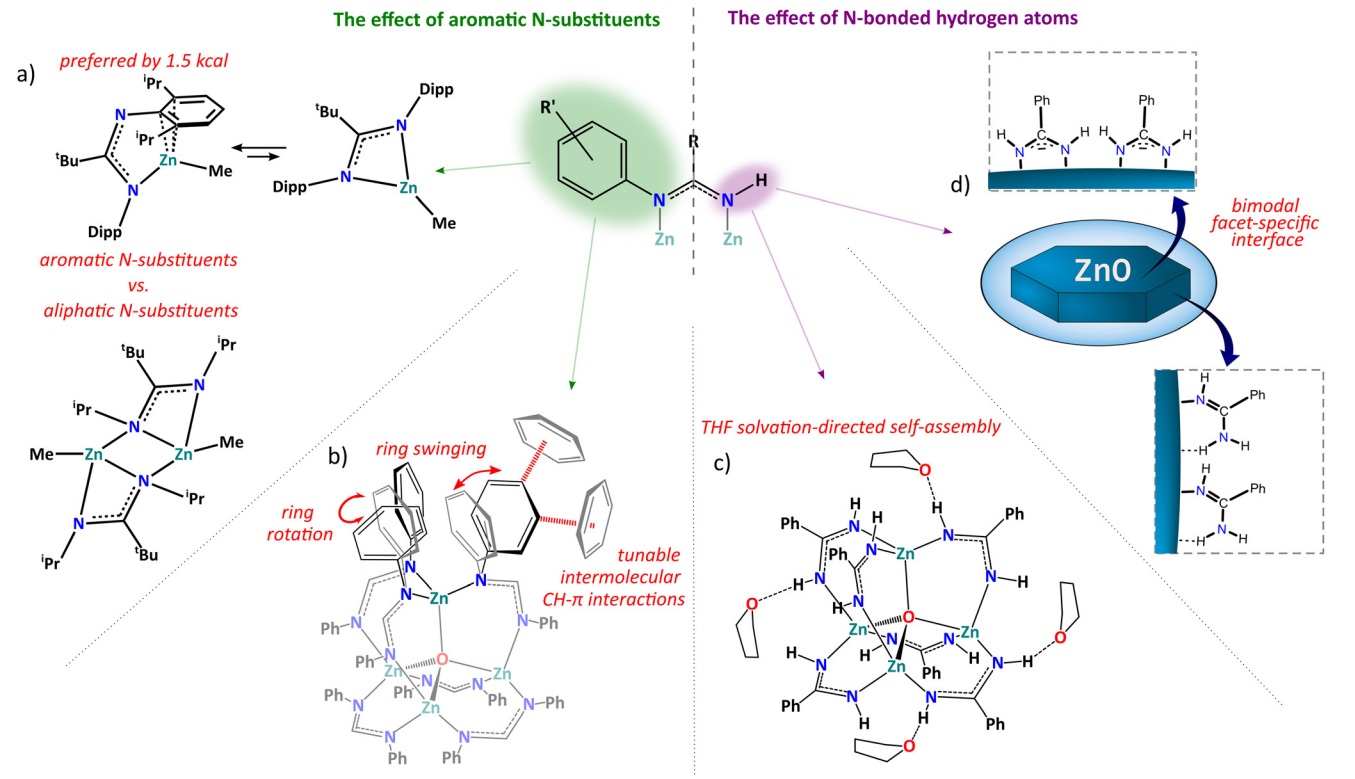


**Fig. 2** Multifaceted role of aromatic *N*-substituents (a and b) and N-bonded hydrogen atoms (c and d) of *N*,*N*′-diaryl and *N*,*N*′-unsubstituted amidinate ligands, respectively, in the structural stabilization and self-assembly of zinc coordination systems.

for intermolecular hydrogen bonds participating in a unique facet-specific bimodal ligands interaction, which led to the preparation of unprecedented nanoplatelets with a controlled thickness (Fig. 2d).[11]

Remarkably, the secondary coordination sphere of the metal environment may not only influence the stabilization of molecular coordination systems but it also is responsible for self-assembly processes mediated by noncovalent interactions. This is well exemplified by tetrahedral zinc–oxido clusters coated by carboxylate[18] or amidinate ligands.[19–21] For example, we observed an interesting solvatomorphism and pressure-induced dynamic behavior of an *N*,*N*′-diphenylformamidinate (dipf) stabilized zinc–oxido cluster, originated in high adaptability of its secondary coordination sphere comprising numerous N-bonded phenyl rings.[20] Interestingly, in this case, the aromatic subunits not only mediated intermolecular CH–π interactions but their conformational movement gradually absorbed compression strain induced by the increasing pressure, which promoted stepwise phase transitions (Fig. 2b) and thus these observations provided a profound understanding of the multistep single-crystal-to-single crystal phase transitions at the atomic level. Other studies also found a profound effect of the introduction of NH units to the proximal secondary coordination sphere of polyhedral zinc–oxido clusters on their crystal packing.[21] In this view, benzamidinate (bza) ligands provided efficient H-donor sites for intermolecular NH···O bonds with the solvating THF molecules leading to a honeycomb supramolecular structure with 1D open-channels (Fig. 2c).

Building on the mentioned above results and our previous experience in studies on the structure and self-assembly of amidinate metal complexes,[11,20,21,34,35] we selected dipf and bza ligands as a model *N*,*N*′-diaryl substituted and *N*,*N*′-unsubstituted NCN scaffold to gain a more in-depth understanding of factors controlling the structure and stability of alkylzinc amidinates. To this aim, we investigated the reactions of dipf–H and bza–H proligands with $ZnR_2$ compounds (R = Me, Et, $^t$Bu) and characterized products containing a systematically modified secondary coordination sphere of the Zn center in both the solid state and solution.

## Results and discussion

### Alkylzincs stabilized by *N*,*N*′-diaryl amidinate ligands

**Reactions of dipf–H with $ZnR_2$ compounds (R = Me, Et).** From equimolar reactions of dipf–H with $ZnR_2$ compounds in toluene we repeatedly isolated crystals of $[R_2Zn_3(dipf)_4]$ (R = Me ($\mathbf{1^{Me}}$) or Et ($\mathbf{1^{Et}}$)) complexes in high yields (Fig. 3). Notably, despite the utilization of stoichiometric amounts of reagents, the isolated products are non-stoichiometric and comprise the ligand-to-alkyl ratio of 2 : 1, which indicates subsequent transformations of the initially formed [RZn(dipf)]-type species. Thus, in order to better understand the $ZnR_2$/dipf-H reaction system and the formation of $\mathbf{1^R}$-type compounds, we performed Diffusion-Ordered NMR spectroscopy (DOSY NMR) experiments on the equimolar reactions of dipf–H with $ZnR_2$ (R = Me, Et) in $d_8$-toluene (for details, see ESI†). Molecular weights of examined species ($MW_{est}$) were estimated utilizing an external calibration curve (ECC) approach with normalized diffusion coefficients, exploiting 1,2,3,4-tetraphenylnaphtalene (TPhN) as an internal reference,[36] and compared with the molecular weights of respective compounds including correction due to the presence of heavy elements ($MW_{corr}$).[37] Analysis revealed two components in the post-reaction mixtures with the $MW_{est}$ of 762 and 66 g mol$^{-1}$, and 761 and 117 g mol$^{-1}$ for methyl- and ethylzinc derivatives, respectively, which indicates the equimolar formation of $[R_2Zn_3(dipf)_4]$-type moieties ($MW_{corr}$ = 746 and 776 g mol$^{-1}$ for R = Me, Et, respectively) and $ZnR_2$ ($MW_{corr}$ = 49 and 79 g mol$^{-1}$ for R = Me, Et, respectively), irrespective of the character of Zn-bonded alkyl group (Fig. S13–S18, and Tables S1–S4†). This suggests that the initially formed $[RZn(dipf)]_x$-type species are relatively unstable and undergo the Schlenk equilibria-mediated ligand scrambling leading to the more thermodynamically stable non-stoichiometric $[R_2Zn_3(dipf)_4]$-type clusters (Fig. 3). Interestingly, we observed a similar ligand rearrangement in our previous studies concerning alkylzinc pyrazolates.[13] However, contrary to the dipf derivatives, the pyrazolate $[EtZnL]_x$-type species formed during the synthesis were stable in solution and undergo ligand scrambling only during the crystallization leading to non-stoichiometric $[Et_2Zn_3L_4]$- or $[Et_2Zn_4L_6]$-type complexes that preserved their structure upon subsequent dissolution.

Complexes $\mathbf{1^{Me}}$ and $\mathbf{1^{Et}}$ can be also easily obtained with almost quantitative yields by the reaction of dipf–H with $ZnR_2$ in a 4 : 3 molar ratio and as received products were characterized by single-crystal X-ray diffraction (SC-XRD), FTIR and NMR spectroscopy, and elemental analysis. Crystal structures examination showed that the molecules of $\mathbf{1^{Me}}$ and $\mathbf{1^{Et}}$ are essentially isostructural but differ in the conformation of the N-bonded aromatic rings in the secondary coordination sphere. Their molecular structure can be described as a combination of two [RZn(dipf)] and one $[Zn(dipf)_2]$ moieties. The core of $\mathbf{1^R}$ comprises three Zn centers with a right triangle geometry (the largest Zn–Zn–Zn angles within the individual complexes are in the range of 88.81(2)–92.55(2)°) (Fig. 4a). All zinc centers exhibit a similar distorted tetrahedral geometry of the coordination sphere, however, the two of them comprised alkyl groups while the last one is bonded only by four amidinate ligands. The $\{Zn_3\}$ core is stabilized by four dipf ligands, two adopting $\mu_2$ coordination and the other two acting as $\mu_3$ bridges (Fig. 4d and e). In the $\mu_2$ coordination mode, both N–Zn bonds are of similar length (1.988(2)–2.055(3) Å) and coplanar with the NCN plane. The $\mu_3$ coordination mode comprises two similar N–Zn distances essentially coplanar with the NCN unit and the perpendicular third one that is significantly longer (the Zn–N lengths of two bonds coplanar with the NCN units and the third perpendicular bond are in the ranges of 2.045(2)–2.073(2) Å and 2.261(2)–2.346(2) Å, respectively). The different character of both donor N centers in $\mu_3$ dipf ligands introduces significant asymmetry to the amidinate group (the

 

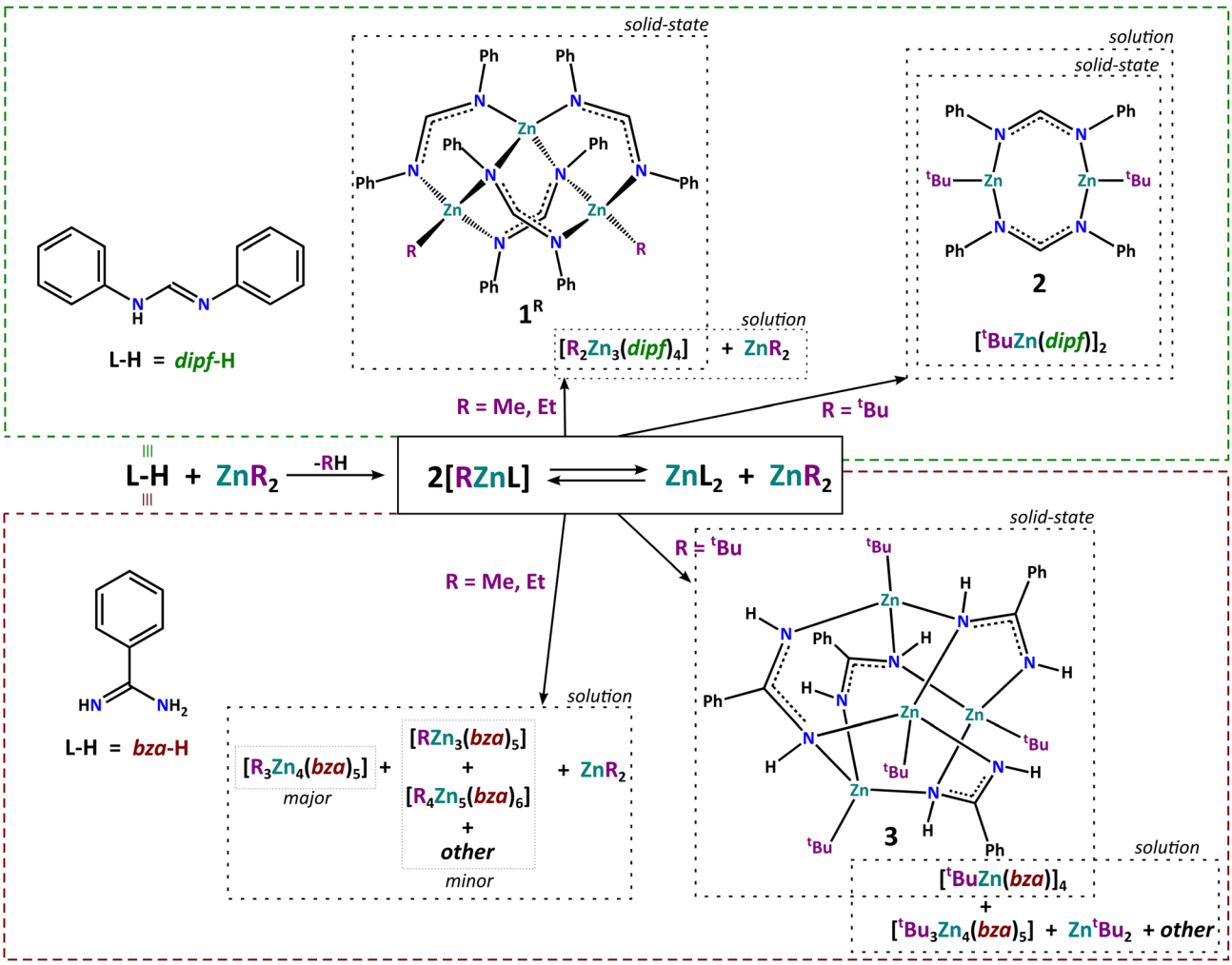


**Fig. 3** Schematic representation of equimolar reactions of the model dipf–H and bza–H proligands with the representative homoleptic organozincs $ZnR_2$ (R = Me, Et, $^t$Bu).

C–N distances to mono- and bi-dentate N centers of the $\mu_3$ ligands are in the ranges of 1.292(4)–1.306(4) Å and 1.348(3)–1.366(4) Å, respectively, while all the C–N distances in the $\mu_2$ ligands are in the range of 1.313(4)–1.328(4) Å). Interestingly, the eight phenyl rings in the secondary coordination sphere of $\mathbf{1}^{\mathbf{Me}}$ and $\mathbf{1}^{\mathbf{Et}}$ complexes are arranged indicating the presence of numerous specific noncovalent interactions. Especially, in $\mathbf{1}^{\mathbf{Me}}$ the phenyl rings seem to form two CH–π : π–π : CH–π systems of cooperative interactions on top and bottom of the triangular core (Fig. 4b; the distances between the ring planes in π–π interactions are about 3.12–3.67 Å and the distances of H atoms to respective ring planes in CH–π interactions are about 2.68–2.94 Å). In turn, $\mathbf{1}^{\mathbf{Et}}$ differs in the conformation of two aromatic rings on the bottom side of the $\{Zn_3\}$ core resulting in CH–π : CH–π : CH–π system of cooperative noncovalent interactions (Fig. 4c; the distance between the ring planes in π–π interaction is about 3.51 Å and the distances of H atoms to respective ring planes in CH–π interactions are about 2.43–2.91 Å). Notably, in solution, the conformation of aromatic rings in both $\mathbf{1}^{\mathbf{Me}}$ and $\mathbf{1}^{\mathbf{Et}}$ is similar to that observed in the crystal structure of $\mathbf{1}^{\mathbf{Me}}$ (*vide infra*) indicating that the system involving two CH–π : π–π : CH–π sets of interactions is likely more thermodynamically favored. Thus, the different conformation of phenyl rings observed in the crystal structure of $\mathbf{1}^{\mathbf{Et}}$ is probably a combined effect of the ethyl group steric hindrance and a specific environment of the close-packed molecules.

Analysis of the NMR spectra indicates that the solid-state molecular structures of $\mathbf{1}^{\mathbf{Me}}$ and $\mathbf{1}^{\mathbf{Et}}$ are essentially preserved in solution. Especially, the $^1$H NMR spectrum of $\mathbf{1}^{\mathbf{Me}}$ in $C_6D_6$ shows two singlets with the same intensity at 8.24 and 7.85 ppm and a complicated set of resonances from the aromatic hydrogen atoms in the range 8.4–5.7 ppm, which confirm the presence of two different forms of dipf ligands (Fig. 5). Furthermore, one of the aromatic resonances, with the relative intensity of 4H, is highly upfield shifted to about 5.7 ppm, which is likely related to the four specific CH–π contacts. This indicates a similar configuration of the aromatic rings to that observed in the crystal structure of $\mathbf{1}^{\mathbf{Me}}$, involving four CH–π interactions. The $^1$H NMR spectrum of $\mathbf{1}^{\mathbf{Et}}$ (Fig. S3†)

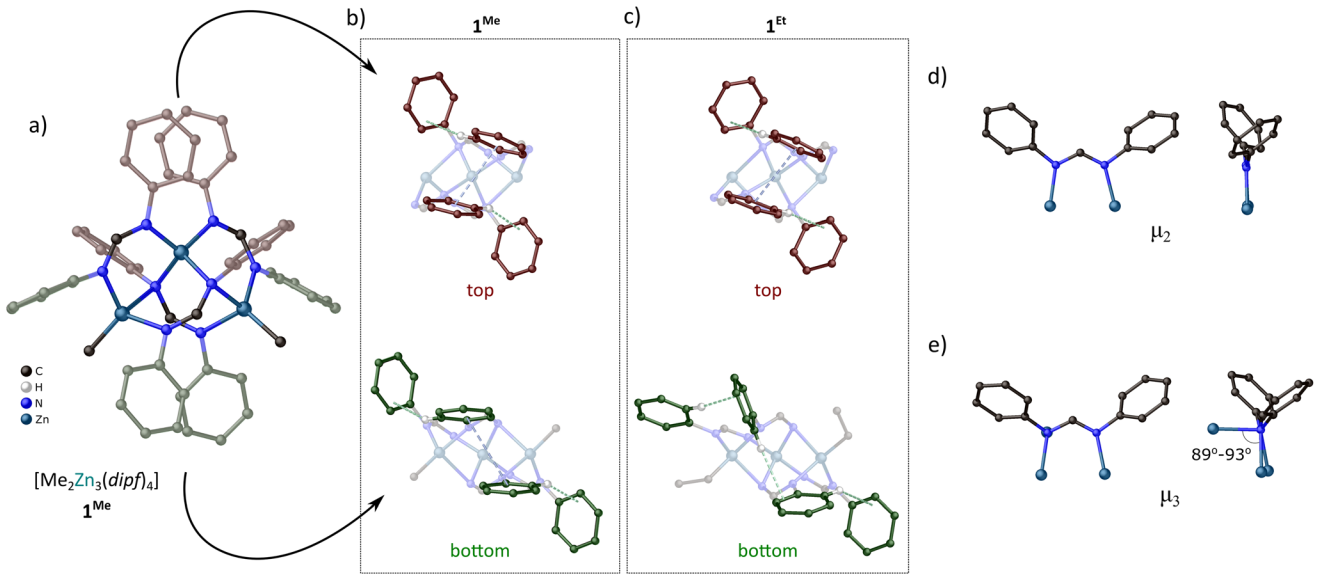


**Fig. 4** Molecular structure of $\mathbf{1^{Me}}$ (a); view on the configuration of aromatic rings on the top and bottom of triangular core in $\mathbf{1^{Me}}$ (b) and $\mathbf{1^{Et}}$ (c); $\mu_2$ (d) and $\mu_3$ (e) coordination modes of dipf ligands in $\mathbf{1^R}$.

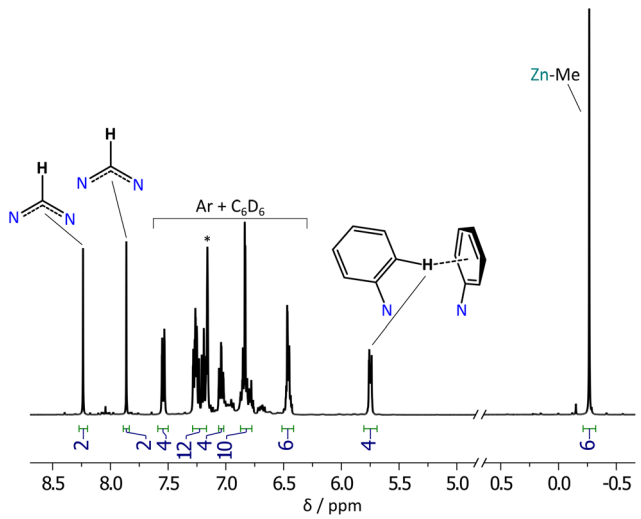


**Fig. 5** $^1$H NMR spectrum of $\mathbf{1^{Me}}$ in $C_6D_6$ solution.

is essentially identical to that of $\mathbf{1^{Me}}$ indicating the same conformation of aromatic rings in the secondary coordination sphere (four specific CH–π contacts based on $^1$H NMR signal intensity).

We note that $\mathbf{1^{Et}}$ was obtained previously by Zhao and coworkers, who studied the effect of steric hindrances in the aromatic rings on the structure of ethylzinc *N*,*N*′-diarylformamidinates.[28] However, the authors didn't consider the role of secondary coordination sphere interactions on its structural stabilization neither their solution behavior. Still, they reviled that introduction of substituents in the *ortho*-position of N-bonded aromatic subunits of amidinate ligands resulted in the stabilization of THF solvated dimers $[EtZnL]_2$·THF, instead of non-stoichiometric trinuclear $[Et_2Zn_3L_4]$-type complexes isolated for *ortho*-unsubstituted ligands. Notably, these *ortho*-substituents not only introduce steric hindrances to the amidinate ligands but also prevent the formation of CH–π interactions described above.

**Reactions of dipf–H with di(*tert*-butyl)zinc.** The equimolar reaction of dipf–H with $Zn(^tBu)_2$ in toluene solution followed by crystallization at 5 °C afforded colorless crystals of $[(^tBu)Zn(dipf)]_2$ (**2**) in a high yield, which were characterized by SC-XRD, NMR and FTIR spectroscopies, and elemental analysis. The molecular structure of **2** consists of two Zn–$^t$Bu moieties connected by two $\mu_2$-bridging amidine anions (Fig. 6a). Both zinc centers adopt a similar almost planar distorted trigonal geometry of coordination sphere composed of two nitrogen atoms of two dipf ligands and one carbon atom of the alkyl group. The Zn–N distances are in the range of 1.980(4)–2.046

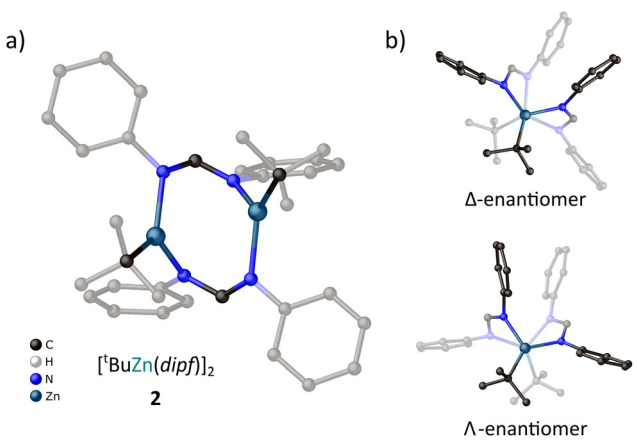


**Fig. 6** Molecular structure of **2** (a), and view along Zn–Zn line on the Δ/Λ conformers (b).

(4) Å, which is similar to that observed for $\mu_2$ bridges in $\mathbf{1}^{Me}$ and $\mathbf{1}^{Et}$. However, contrary to $[R_2Zn_3(dipf)_4]$-type complexes, in the case of **2**, the Zn–N bonds within individual $\mu_2$ ligands are not coplanar but significantly diverge from the N–C–N planes (the Zn–N–N–Zn torsion angles are in the range of 42.9(2)–54.3 (2)°). The twisting of amidinate groups results in a synclinal conformation of **2** along the Zn–Zn line, which is likely an effect of steric hindrance between the $^t$Bu groups. Interestingly, this specific conformation induces chirality in the system, and the crystals of **2** are composed of a racemic mixture of *Δ*- and *Λ*-enantiomers (Fig. 6b).

The $^1$H and $^{13}$C NMR spectra of **2** in $C_6D_6$ solution are consistent with the structure observed in solid-state indicating the presence of only one form of dipf ligand (Fig. S5 and S6†). The $^1$H NMR spectrum shows a singlet at 7.68 ppm, three multiplets in the range of 6.8–7.0 ppm, and an intensive singlet at 1.47 ppm, associated with amidinate, aromatic, and $^t$Bu hydrogen atoms, respectively. In turn, the $^{13}$C NMR spectrum shows single resonances at 161.6 and 148.5 ppm associated with amidinate and tertiary aromatic carbon atoms of the single dipf ligand. Further three signals at 129.9, 124.3, 122.0 ppm, and two signals at 33.4 and 24.8 ppm are associated with the rest of the phenyl group carbon atoms and $^t$Bu group, respectively.

The above results indicate that the steric hindrances in the proximity of metal centers play a significant role in the stabilization of $[RZn(L)]_x$-type amidinate species. Thus, while the methyl and ethyl dipf derivatives selectively stabilized non-stoichiometric $[Et_2Zn_3L_4]$-type coordination systems, the more sterically demanding *tert*-butylzinc analogue selectively leads to the dimeric $[(^t$Bu)Zn(dipf)$]_2$ complex (Fig. 3). This is in line with results obtained by Zhao and coworkers, who demonstrated that the dimeric $[EtZn(L)]_2$·THF-type structures were favored over the non-stoichiometric $[Et_2Zn_3(L)_4]$-type complexes in the case of amidinate ligands with sterically demanding N-bonded aryl subunits.[28] This emphasizes that the steric hindrance of both organic ligands and alkylzinc groups are important factors competing with secondary coordination sphere noncovalent interactions in the stabilization of the molecular structure of organometallic complexes.

### Alkylzincs stabilized by *N,N′*-unsubstituted amidinate ligands

**Reactions of bza–H with $ZnR_2$ compounds (R = Me, Et).** Equimolar reactions of bza–H with $ZnR_2$ (R = Me, Et) in toluene afforded colorless solutions. Unfortunately, all attempts to isolate well-defined crystal products from these reactions failed, affording in white precipitates that were characterized by $^1$H and $^{13}$C NMR spectroscopy. The NMR spectra of the isolated methyl- and ethylzinc derivatives in $d_8$-toluene are similar and indicate the complicated structure of these products. Especially, the resonances of N-bonded hydrogen atoms in the $^1$H NMR spectra are split into sets of signals in the range of 4.0–6.2 ppm, which indicate a diverse chemical environment around amidinate functional groups (Fig. 7 and S9†). Furthermore, one of these signals is significantly downfield shifted to about 6.1 ppm, which may be associated with the formation of some NH···X hydrogen interactions. In turn,

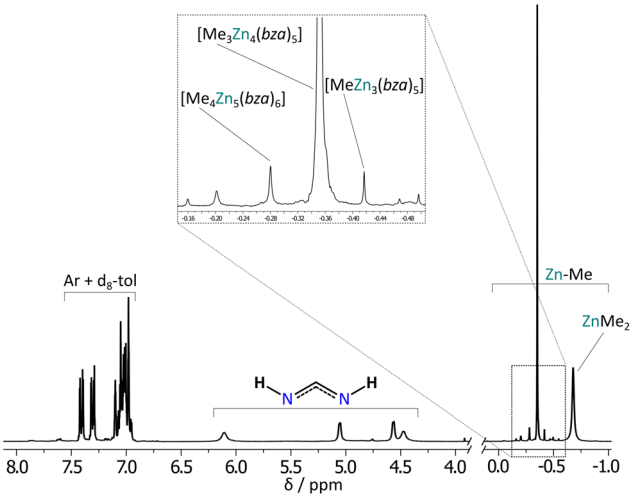


**Fig. 7** $^1$H NMR spectrum from the equimolar reaction of bza–H with $ZnMe_2$ in $d_8$-toluene solution.

multiple resonances from the zinc-bonded alkyl groups also indicate the presence of several nonequivalent alkylzinc moieties. Finally, multiple signals form amidinate and quaternary aromatic carbon atoms in $^{13}$C NMR spectra indicate the presence of at least three various forms of bza ligands (Fig. S8 and S10†). Interestingly, the estimated bza to alkylzinc groups ratio based on respective peak intensities in $^1$H NMR spectra (Fig. S7 and S9†) is about 1 : 0.3 and 1 : 0.4 for methyl- and ethylzinc derivatives, respectively, which suggests the formation of non-stoichiometric complexes with an excess of bza ligands compared to alkylzinc groups.

To gain more insights into the bza–H/$ZnR_2$ reaction system, we performed DOSY NMR analysis of the post-reaction mixtures in $d_8$-toluene (for details, see ESI†). Analysis revealed the presence of two main components with the $MW_{est}$ of 609 and 86 g mol$^{-1}$, and 653 and 124 g mol$^{-1}$ for methyl- and ethylzinc derivatives, respectively, which indicates the formation of $[R_3Zn_4(bza)_5]$-type moieties ($MW_{corr}$ = 610 and 655 g mol$^{-1}$ for R = Me, Et, respectively) and $ZnR_2$ ($MW_{corr}$ = 49 and 79 g mol$^{-1}$ for R = Me, Et, respectively) (Fig. S19–S24, and Tables S5–S8†). Furthermore, the $^1$H NMR spectra show several additional signals in the aliphatic region that suggest the formation of minor products, which in the case of methylzinc derivative can be assigned to other non-stoichiometric complexes like $[Me_4Zn_5(bza)_6]$ ($MW_{est}$ = 735, $MW_{corr}$ = 741 g mol$^{-1}$) and $[MeZn_3(bza)_6]$ ($MW_{est}$ = 567, $MW_{corr}$ = 561 g mol$^{-1}$) moieties (Fig. 7). Thus, the data indicates a low selectivity of bza ligands in the stabilization of specific alkylzinc complexes. As in the case of methyl- and ethylzinc derivatives of dipf–H, the initially formed benzamidinate $[RZn(bza)]_x$-type species are essentially unstable and undergo fast Schlenk equilibria-mediated ligand scrambling leading to more thermodynamically stable non-stoichiometric coordination systems (Fig. 3). However, the bza ligand provide less specific stabilization than dipf one resulting in a mixture of various non-stoichiometric complexes instead of one dominant form. Notably, bza ligands create

little steric hindrance, thus in this case, the structure of non-stoichiometric alkylzinc systems is likely stabilized by noncovalent interactions involving the NH groups in the secondary coordination sphere.

**Reactions of bza–H with di(*tert*-butyl)zinc.** Contrary to the methyl- and ethylzinc derivatives, a yellowish toluene solution obtained from the reaction of bza–H with $Zn(^tBu)_2$ afforded high-quality single crystals of a tetrameric complex $[(^tBu)Zn(bza)]_4$ (**3**) in a moderate yield after 5 days storage at 5 °C. Complex **3** was characterized by SC-XRD, NMR and FTIR spectroscopy, and elemental analysis. The molecular structure of **3** comprises a $\{ZnNZnNCN\}_4$ core with the $\bar{4}$ symmetry built by four fused by edges Zn–N–Zn–NCN–metallamacrocycles (Fig. 8a). The phenyl rings of bza ligands are directed above and below the barrel-like core, while the zinc-bonded alkyl groups occupy the side positions around it. All Zn centers are symmetrically equivalent adopting the same slightly distorted geometry of the coordination sphere. Four bza ligands exhibit the same $\mu_3$ coordination mode resulting in the diversification of the N–C bonds within the amidinate functionality (the N–C distances are 1.298(2) and 1.360(2) Å to the monodentate and bridging N centers, respectively). This $\mu_3$ coordination mode of bza ligands differs significantly from that observed for dipf ligands in the complexes $\mathbf{1}^{\mathbf{R}}$ (*vide supra*). Particularly, in the $\mu_3$-bza ligands both Zn–N bonds to the bridging N center substantially deviate from the NCN plane of amidinate group and the angle between them is 105.25(7)° (Fig. 8b), while in the $\mu_3$-dipf ligands, two of the Zn centers are essentially coplanar with the NCN plane and the third Zn center is coordinated almost perpendicular to them (Fig. 4e). Moreover, the Zn–N distances in **3** are 2.000(2), 2.083(1), and 2.165(2) Å to the monodentate and bridging N centers, respectively, exhibiting much smaller diversification than in $\mathbf{1}^{\mathbf{R}}$.

Interestingly, NMR spectra analysis reviled that upon dissolution in $d_8$-toluene complex **3** undergoes ligand scrambling with the formation of various forms of *tert*-buthylzinc benzamidinates (see ESI, Fig. S25 and S26†). Both $^1H$ and $^{13}C$ NMR spectra of **3** show multiple signals in the range of 1.7–0.7 ppm and 37–17 ppm, respectively, indicating the presence of $^t$Bu groups with various chemical environments (Fig. 9 and S12†). In turn, multiple signals in the ranges of 182–172 ppm and 144–136 ppm in the $^{13}C$ NMR spectrum characteristic for the amidinate and tertiary aromatic carbon atoms, respectively, suggest at least four different coordination modes of bza ligands. $^1H$ DOSY NMR analysis shows that the three most intensive resonances in the region of alkyl groups, at *ca.* 1.40, 1.26, and 1.07 ppm, belong to various *tert*-butylzinc complexes with estimated molecular weights of 696, 746, and 158 g mol$^{-1}$ matching well to the parent tetramer $[(^tBu)Zn(bza)]_4$ ($MW_{corr}$ = 706 g mol$^{-1}$), a non-stoichiometric complex $[(^tBu)_3Zn_4(bza)_5]$ ($MW_{corr}$ = 744 g mol$^{-1}$), and $Zn(^tBu)_2$ ($MW_{corr}$ = 139 g mol$^{-1}$), respectively (Fig. S25, S26 and Tables S9, S10†). However, the presence of other less intensive signals in this region indicates a more complex mixture of products likely resulted in complicated equilibria in solution. Note, that several attempts to obtain crystals of $[(^tBu)_3Zn_4(bza)_5]$ by crystallization in various conditions (temperature, different solvents) yielded selectively the tetrameric complex **3**, which is likely the most thermodynamically stable (or the least soluble) form of the *tert*-butylzinc bza derivatives. This is in agreement with the result obtained for the analogous dipf derivatives, indicating that the sterically demanding *tert*-butyl substituents on zinc centers favor the formation of $[RZnL]_x$-type species, which is also strongly affected by a combination of steric and electronic effects mediated by the N-bonded substituents.

The above results show the unique ability of bza ligand for the stabilization of a vast array of non-stoichiometric alkylzinc complexes, including $[RZn_3(bza)_5]$-, $[R_3Zn_4(bza)_5]$-, and

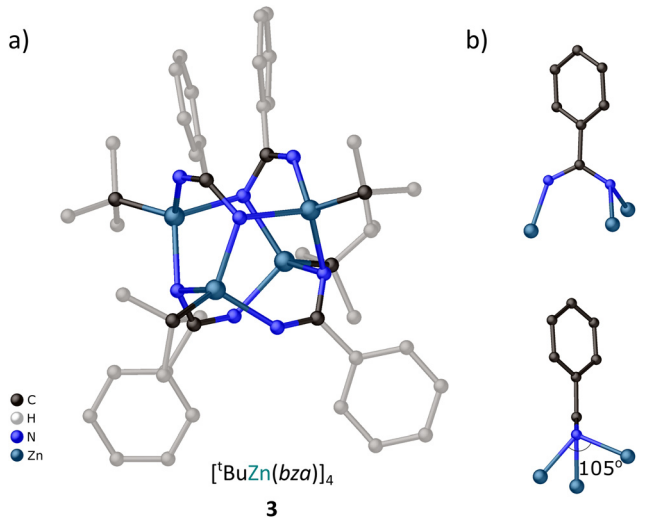


3

Fig. 8 Molecular structure of **3** and $\mu_3$ coordination mode of bza ligands.

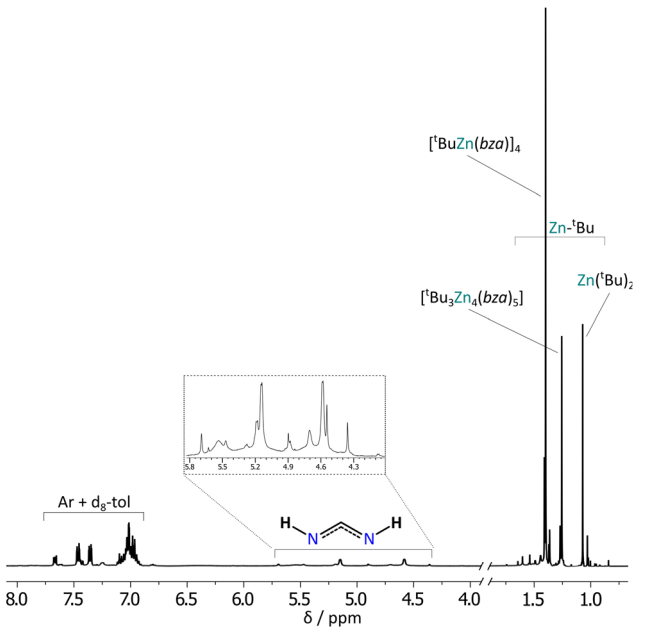


Fig. 9 $^1H$ NMR spectrum of **3** in $d_8$-toluene solution.

$[R_4Zn_5(bza)_6]$-type systems. To the best of our knowledge, non-stoichiometric trinuclear and tetranuclear alkylzinc complexes were so far characterized only as $[R_2Zn_3L_4]$ and $[R_2Zn_4L_6]$-type coordination systems (either as linear spiro-type structures,[13,15] or clusters with the trigonal-, or square-planar arrangement of metal centers[28,38]) and $[RZn_3L_5]$- as well as $[R_3Zn_4L_5]$-type structural motives remain unexplored. In turn, an interesting $[R_4Zn_5L_6]$-type structure was characterized for an ethylzinc acetate, comprising a central six-coordinate inorganic Zn ion in a tetrahedral surrounding of four alkylzinc centers connected by six $\mu_3$-acetate ligands.[39] A similar structure may be adapted by $[R_4Zn_5(bza)_6]$-type complexes.

# Conclusion

In conclusion, we investigated the solid state and solution structure of a series of alkylzinc complexes incorporating *N*,*N*′-diaryl substituted and *N*,*N*′-unsubstituted amidinate ligands. We found that $[RZnL]_x$-type amidinate moieties are essentially unstable and tend to undergo ligand scrambling reactions according to Schlenk equilibria leading to more thermodynamically stable non-stoichiometric coordination systems, like $[R_2Zn_3L_4]$- and $[R_3Zn_4L_5]$-type complexes among others. This process is significantly influenced by the size of alkylzinc species and more sterically demanding *tert*-butyl groups favor the stabilization of the $[RZnL]_x$-type system. Interestingly, while the dip-based complexes maintain their solid-state structure in solution, the dissolution of alkylzinc compounds stabilized by bza ligands leads to complicated mixtures of moieties with various stoichiometries. Importantly, the crystallographic and spectroscopic investigations indicate that the interplay between primary and secondary coordination spheres is an important factor controlling the character of resulting products. Moreover, as far as we know, we presented the first systematic characterization of alkylzinc systems stabilized by *N*,*N*′-unsubstituted amidinate ligands. The results provide a better understanding of the factors controlling the structure and stability of alkylzinc amidinates and shed new light on their complex behavior in solution, which in the future may contribute to the development of new efficient reaction systems.

# Experimental section

### General remarks

Organometallic reagents were handled under a nitrogen atmosphere by using the standard Schlenk technique. Dimethylzinc (ABCR), diethylzinc (ABCR), bza–H (Sigma-Aldrich), and dipf–H (ABCR) were purchased from commercial vendors and used as received. Di-*tert*-butylzinc was synthesized according to a literature procedure[40] and purified by careful sublimation in the dark. All solvents were purified and dried using MBraun Solvent Purification System (SPS). The standard NMR and FTIR spectra were acquired on Bruker AVANCE III HD (400 MHz) and Bruker-Tensor II (ATR) spectrometers, respectively. The DOSY NMR experiments were carried out on Bruker AVANCE II (300 MHz) spectrometer. Elemental analyses were performed on the Elementar VarioMicro Cube analyzer.

### Synthesis of $\mathbf{1^{Me}}$

A solution of $ZnMe_2$ in hexane (2 M, 1.5 mL, 3 mmol) was added to a suspension of dipf–H (784 mg, 4 mmol) in toluene (10 mL) cooled to −78 °C. The reaction mixture was stirred at room temperature for 4 h and then crystalized at 5 °C with the addition of hexane to give high-quality colorless crystals of $\mathbf{1^{Me}}$ (isolated yield 86%, 866 mg). Alternatively, the solvent can be removed under vacuum to give the product as a white crystalline powder in a practically quantitative yield. Note, that similar reactions with 1 : 1 and 2 : 1 $ZnMe_2$ to dipf–H molar ratio followed by crystallization at 5 °C also give high-quality colorless crystals of $\mathbf{1^{Me}}$ (yield 76%, 765 mg, and 79%, 796 mg for 1 : 1 and 2 : 1 molar ratio, respectively). $^1$H NMR ($C_6D_6$, 400 MHz): $\delta$ = 8.24 (s, 2H, NC(H)N), 7.86 (s, 2H, NC(H)N), 7.52 (d, 4H, Ar), 7.34–6.72 (m, 26H, Ar), 6.47 (m, 6H, Ar), 5.75 (d, 4H, Ar), −0.27 (s, 6H, $CH_3$); $^{13}$C NMR ($C_6D_6$, 100 MHz): $\delta$ = 169.5, 166.3, 150.8, 150.1, 149.5, 149.0, 129.8, 129.6, 129.0, 125.4, 125.2, 124.8, 124.7, 124.5, 124.4, 123.9, 123.7, −10.5; FTIR (ATR, cm$^{-1}$): 3056 (w), 3029 (w), 2897 (w), 2834 (w), 1610 (m), 1595 (w), 1554 (s), 1484 (s), 1450 (w), 1366 (m), 1359 (s), 1213 (s), 1080 (m), 1027 (m), 993 (s), 772 (s), 756 (s), 694 (s), 648 (m), 526 (s). Elemental analysis (%) calcd for $C_{54}H_{50}Zn_3N_8$: C 64.40, H 5.00, N 11.13; found: C 64.43, H 4.91, N 11.09.

### Synthesis of $\mathbf{1^{Et}}$

The procedure was similar to that described for $\mathbf{1^{Me}}$. Using $ZnEt_2$ in hexane (2 M, 1.5 mL, 3 mmol) and dipf–H (784 mg, 4 mmol) compound $\mathbf{1^{Et}}$ was obtained as colorless crystals after crystallization at 5 °C (isolated yield: 921 mg, 89%). $^1$H NMR ($C_6D_6$, 400 MHz): $\delta$ = 8.36 (s, 2H, NC(H)N), 7.85 (s, 2H, NC(H)N), 7.51 (d, 4H, Ar), 7.25–6.75 (m, 26H, Ar), 6.45 (m, 6H, Ar), 5.72 (d, 4H, Ar), 1.19 (t, 6H, $CH_3$), 0.50 (q, 4H, $CH_2$); $^{13}$C NMR ($C_6D_6$, 100 MHz): $\delta$ = 168.5, 166.0, 150.6, 149.8, 149.2, 148.9, 129.4, 129.3, 128.8, 125.0, 124.6, 124.0, 123.9, 123.6, 123.3, 13.5, 2.7; FTIR (ATR, cm$^{-1}$): 3056 (w), 3029 (w), 2889 (w), 2849 (w), 1609 (m), 1557 (s), 1486 (s), 1451 (w), 1352 (s), 1296 (m), 1209 (s), 1078 (w), 1028 (w), 989 (m), 770 (m), 755 (s), 692 (s), 644 (m), 608 (m), 522 (s). Elemental analysis (%) calcd for $C_{56}H_{54}Zn_3N_8$: C 64.97, H 5.26, N 10.82; found: C 65.04, H 5.13, N 10.75.

### Synthesis of 2

A solution of $Zn(^tBu)_2$ in hexane (0.8 M, 1.25 mL, 1 mmol) was added to a suspension of dipf–H (196 mg, 1 mmol) in toluene (4 mL) cooled to −15 °C. Then the reaction mixture was stirred at room temperature for 4 h and crystalized at 5 °C with the addition of hexane to give high-quality colorless crystals of **2** (isolated yield 289 mg, 91%,). $^1$H NMR ($C_6D_6$, 400 MHz): $\delta$ = 7.68 (s, 2H, NC(H)N), 7.09 (t, 8H, mAr), 6.92 (t, 4H, pAr), 6.84 (d, 8H, oAr), 1.47 (s, 18H, *t*Bu); $^{13}$C NMR ($C_6D_6$, 100 MHz): $\delta$ = 161.6, 148.5, 129.9, 124.3, 122.0, 33.4, 24.8; FTIR (ATR, cm$^{-1}$):

3056 (w), 3023 (w), 2931 (w), 2916 (w), 2810 (m), 1661 (m), 1604 (m), 1547 (s), 1537 (s), 1484 (s), 1406 (m), 1320 (s), 1220 (s), 1080 (m), 977 (s), 929 (m), 810 (m), 766 (s), 756 (s), 690 (s), 649 (m), 523 (m). Elemental analysis (%) calcd for $C_{34}H_{40}Zn_2N_4$: C 64.26, H 6.34, N 8.82; found: C 64.35, H 6.30, N 8.75.

### Synthesis of methyl- and ethylzinc derivatives of bza

A solution of the corresponding $ZnR_2$ in hexane (2 M, 1 mL, 2 mmol) was added to a solution of bza–H (240 mg, 2 mmol) in toluene (7 mL) cooled to −78 °C. The reaction mixture was stirred at room temperature for 4 h. Crystallization at 5 °C with the addition of hexane afforded white precipitates that were characterized by $^1$H and $^{13}$C NMR, and FTIR spectroscopy. Methylzinc derivative: $^1$H NMR ($d_8$-tol, 400 MHz): $\delta$ = 7.90–6.66 (m, Ar), 6.28–3.96 (m, 2H, NH), −0.07–(−0.65) (m, 0.9H, MeZn); $^{13}$C NMR ($d_8$-tol, 100 MHz): $\delta$ = 184.4, 179.4, 147.0, 144.8, 136.1–127.9, −10.1; FTIR (ATR, cm$^{-1}$): 3053 (w), 3020 (w), 2886 (w), 2813 (w), 1590 (s), 1543 (s), 1539 (s), 1510 (s), 1470 (s), 1437 (s), 1269 (s), 1073 (m), 1027 (m), 922 (m), 785 (m), 732 (m), 693 (s), 671 (s), 614 (s), 482 (s). Ethylzinc derivative: $^1$H NMR ($d_8$-tol, 400 MHz): $\delta$ = 7.74–6.87 (m, Ar), 6.28–4.29 (m, 2H, NH), 1.97–1.48 (m, 1.2H, $CH_3$), 0.77–0.40 (m, 0.8H, $CH_2$Zn); $^{13}$C NMR ($d_8$-tol, 100 MHz): $\delta$ = 180.5, 176.0, 174.3, 148.6, 143.0, 140.8, 132.0–123.9, 14.6, −0.3; FTIR (ATR, cm$^{-1}$): 3053 (w), 3023 (w), 2916 (w), 2876 (m), 2838 (m), 1590 (s), 1540 (s), 1509 (s), 1467 (s), 1437 (s), 1266 (s), 1073 (m), 1027 (m), 922 (m), 786 (m), 732 (m), 693 (s), 671 (s), 589 (m), 487 (s).

### Synthesis of 3

A solution of Zn($^t$Bu)$_2$ in hexane (0.8 M, 1.25 mL, 1 mmol) was added to a solution of bza–H (120 mg, 1 mmol) in toluene (5 mL) cooled to −15 °C. The yellowish reaction mixture was stirred at room temperature for 4 h and then crystalized at 5 °C with the addition of hexane to give high-quality colorless crystals of **3** (yield 64%, 155 mg). $^1$H NMR ($d_8$-tol, 400 MHz): $\delta$ = 7.71–6.87 (m, 5H, Ar), 5.75–4.25 (m, 2H, NH), 1.48–0.96 (m, 9H, $t$Bu); $^{13}$C NMR ($d_8$-tol, 100 MHz): $\delta$ = 181.6, 180.8, 175.9, 142.5, 139.61, 138.5, 137.4, 131.7–124.19, 35.5–34.1, 21.9–19.4; FTIR (ATR, cm$^{-1}$): 3056 (w), 3023 (w), 2909 (m), 2850 (m), 2793 (s), 1592 (s), 1552 (s), 1508 (s), 1455 (s), 1432 (s), 1266 (s), 1219 (m), 1102 (m), 1027 (m), 842 (m), 809 (m), 788 (m), 747 (m), 697 (s), 671 (s), 488 (m). Elemental analysis (%) calcd for $C_{44}H_{64}Zn_4N_8$: C 54.68, H 6.67, N 11.59; found: C 54.70, H 6.72, N 11.69.

### NMR experiments

In all cases, a solution of the corresponding $ZnR_2$ in $d_8$-toluene (1 M, 0.2 mL, 0.2 mmol) was added to a solution of dipf–H or bza–H (0.2 mmol) in $d_8$-toluene (1 mL) cooled to −78 °C. The reaction mixture was stirred at room temperature for 4 h and moved to NMR tubes equipped with J. Young valve for analysis. To the samples for DOSY NMR 1,2,3,4-tetraphenylnaphthalene (10 mg, 0.02 mmol) was added as an internal standard.

### X-Ray structure determination

The crystals were selected under Paratone–N oil, mounted on the nylon loops and positioned in the cold stream on the diffractometer. The X-ray data for complexes $\mathbf{1^{Me}}$, **2**, and **3** were collected at 100(2) K on a SuperNova Agilent diffractometer using MoKα radiation ($\lambda$ = 0.71073 Å). The data were processed with CrysAlisPro.[41] The X-ray data for complex $\mathbf{1^{Et}}$ were collected at 100(2) K on a Nonius KappaCCD diffractometer using MoKα radiation ($\lambda$ = 0.71073 Å). The data were processed with HKL2000.[42] Structures were solved by direct methods using the SHELXT program and were refined by full-matrix least–squares on $F^2$ using the program SHELXL.[43] All non-hydrogen atoms were refined with anisotropic displacement parameters. Hydrogen atoms were added to the structure model at geometrically idealized coordinates and refined as riding atoms.

Crystal data for $\mathbf{1^{Me}}$ (CCDC 2220050†), $C_{54}H_{50}N_8Zn_3$: $M$ = 1007.13, monoclinic, space group $P2_1/n$ (no. 14), $a$ = 18.5634(3) Å, $b$ = 24.5535(4) Å, $c$ = 22.3642(4) Å, $\beta$ = 107.018(2)°, $U$ = 9747.2(3) Å$^3$, $Z$ = 8, $F$(000) = 4160, $D_c$ = 1.373 g cm$^{-3}$, $\mu$(Mo-Kα) = 1.509 mm$^{-1}$, $\theta_{max}$ = 27.000°, 21 042 unique reflections. Refinement converged at $R_1$ = 0.0640, w$R_2$ = 0.0844 for all data ($R_1$ = 0.0407, w$R_2$ = 0.0763 for 16 019 reflections with $I_o > 2\sigma(I_o)$). The goodness-of-fit on $F^2$ was equal 1.044.

Crystal data for $\mathbf{1^{Et}}$ (CCDC 2220051†), $C_{56}H_{54}N_{16}Zn_6$: $M$ = 1035.18, monoclinic, space group $P2_1/n$ (no. 14), $a$ = 11.7300(2) Å, $b$ = 13.4060(3) Å, $c$ = 31.6940(7) Å, $\beta$ = 100.5050(10) °, $U$ = 4900.42(18) Å$^3$, $Z$ = 4, $F$(000) = 2144, $D_c$ = 1.403 g cm$^{-3}$, $\mu$(Mo-Kα) = 1.503 mm$^{-1}$, $\theta_{max}$ = 27.419°, 11 110 unique reflections. Refinement converged at $R_1$ = 0.0789, w$R_2$ = 0.0957 for all data ($R_1$ = 0.0474, w$R_2$ = 0.0883 for 8048 reflections with $I_o > 2\sigma(I_o)$). The goodness-of-fit on $F^2$ was equal to 1.039.

Crystal data for **2** (CCDC 2220052†), $C_{34}H_{40}N_4Zn_2$: $M$ = 635.44, monoclinic, space group $P21$ (no. 4), $a$ = 15.2257(2) Å, $b$ = 22.1226(2) Å, $c$ = 19.5545(2) Å, $\beta$ = 104.4370(10)°, $U$ = 6378.59(12) Å$^3$, $Z$ = 8, $F$(000) = 2656, $D_c$ = 1.323 g cm$^{-3}$, $\mu$(Mo-Kα) = 1.532 mm$^{-1}$, $\theta_{max}$ = 25.981°, 18 795 unique reflections. Refinement converged at $R_1$ = 0.0469, w$R_2$ = 0.1148 for all data ($R_1$ = 0.0434, w$R_2$ = 0.1111 for 17 490 reflections with $I_o > 2\sigma(I_o)$). The goodness-of-fit on $F^2$ was equal to 1.025.

Crystal data for **3** (CCDC 2220053†), $C_{44}H_{64}N_8Zn_4$: $M$ = 966.51, tetragonal, space group $I4_1/a$ (no. 88), $a$ = 19.5833(3) Å, $b$ = 19.5833(3) Å, $c$ = 12.0916(3) Å, $U$ = 4637.20(18) Å$^3$, $Z$ = 4, $F$(000) = 2016, $D_c$ = 1.384 g cm$^{-3}$, $\mu$(Mo-Kα) = 2.083 mm$^{-1}$, $\theta_{max}$ = 29.148°, 2758 unique reflections. Refinement converged at $R_1$ = 0.0360, w$R_2$ = 0.0682 for all data ($R_1$ = 0.0286, w$R_2$ = 0.0651 for 2399 reflections with $I_o > 2\sigma(I_o)$). The goodness-of-fit on $F^2$ was equal to 1.064.

## Conflicts of interest

There are no conflicts to declare.

## Acknowledgements

We acknowledge the Foundation for Polish Science Team Programme co-financed by the European Union under the European Regional Development Fund POIR.04.04.00-00-20C6/

16-00 (TEAM/2016-2/14) and the National Science Centre (Grant MAESTRO 11, No. 2019/34/A/ST5/00416) for financial support.



## References

1 K. Soai and S. Niwa, *Chem. Rev.*, 1992, **92**, 833–856.
2 J. T. B. H. Jastrzebski, J. Boersma and G. van Koten, in *PATAI'S Chemistry of Functional Groups*, John Wiley & Sons, Ltd, Chichester, UK, 2009.
3 M. Kubisiak, K. Zelga, W. Bury, I. Justyniak, K. Budny-Godlewski, Z. Ochal and J. Lewiński, *Chem. Sci.*, 2015, **6**, 3102–3108.
4 A. Raheem Keeri, I. Justyniak, J. Jurczak and J. Lewiński, *Adv. Synth. Catal.*, 2016, **358**, 864–868.
5 S. V. Athavale, A. Simon, K. N. Houk and S. E. Denmark, *Nat. Chem.*, 2020, **12**, 412–423.
6 H. Pellissier, *Coord. Chem. Rev.*, 2021, **439**, 213926.
7 Y. Geiger, *Chem. Soc. Rev.*, 2022, **51**, 1206–1211.
8 M. Terlecki, M. Wolska-Pietkiewicz and J. Lewiński, *in Nanomaterials Via Single-Source Precursors*, ed. A. W. Apblett, A. R. Barron and A. F. Hepp, Elsevier, 2022, pp. 245–280.
9 K. L. Orchard, M. S. P. Shaffer and C. K. Williams, *Chem. Mater.*, 2012, **24**, 2443–2448.
10 D. Lee, M. Wolska-Pietkiewicz, S. Badoni, A. Grala, J. Lewiński and G. De Paëpe, *Angew. Chem., Int. Ed.*, 2019, **58**, 17163–17168.
11 M. Terlecki, S. Badoni, M. K. Leszczyński, S. Gierlotka, I. Justyniak, H. Okuno, M. Wolska-Pietkiewicz, D. Lee, G. De Paëpe and J. Lewiński, *Adv. Funct. Mater.*, 2021, **31**, 2105318.
12 J. Rio, L. Perrin and P.-A. Payard, *Eur. J. Org. Chem.*, 2022, e202200906.
13 S. Komorski, M. K. Leszczyński, I. Justyniak and J. Lewiński, *Dalton Trans.*, 2020, **49**, 17388–17394.
14 E. M. Hanada, K. Jess and S. A. Blum, *Chem. – Eur. J.*, 2020, **26**, 15094–15098.
15 Ł. Mąkolski, V. Szejko, K. Zelga, A. Tulewicz, P. Bernatowicz, I. Justyniak and J. Lewiński, *Chem. – Eur. J.*, 2021, **27**, 5666–5674.
16 M. Dochnahl, K. Löhnwitz, J. W. Pissarek, M. Biyikal, S. R. Schulz, S. Schön, N. Meyer, P. W. Roesky and S. Blechert, *Chem. – Eur. J.*, 2007, **13**, 6654–6666.
17 Ł. Mąkolski, K. Zelga, R. Petrus, D. Kubicki, P. Zarzycki, P. Sobota and J. Lewiński, *Chem. – Eur. J.*, 2014, **20**, 14790–14799.
18 W. Bury, I. Justyniak, D. Prochowicz, A. Rola-Noworyta and J. Lewiński, *Inorg. Chem.*, 2012, **51**, 7410–7414.
19 W. Bury, A. M. Walczak, M. K. Leszczyński and J. A. R. Navarro, *J. Am. Chem. Soc.*, 2018, **140**, 15031–15037.
20 M. Terlecki, S. Sobczak, M. K. Leszczyński, A. Katrusiak and J. Lewiński, *Chem. – Eur. J.*, 2021, **27**, 13757–13764.
21 M. Terlecki, I. Justyniak, M. K. Leszczyński and J. Lewiński, *Commun. Chem.*, 2021, **4**, 133.
22 J. Lewiński, W. Sliwiński, M. Dranka, I. Justyniak and J. Lipkowski, *Angew. Chem., Int. Ed.*, 2006, **45**, 4826–4829.
23 T. Pietrzak, I. Justyniak, M. Kubisiak, E. Bojarski and J. Lewiński, *Angew. Chem., Int. Ed.*, 2019, **58**, 8526–8530.
24 T. Chlupatý and A. Růžička, *Coord. Chem. Rev.*, 2016, **314**, 103–113.
25 F. T. Edelmann, in *Advances in Organometallic Chemistry*, 2008, vol. 57, pp. 183–352.
26 A. Baishya, L. Kumar, M. K. Barman, H. S. Biswal and S. Nembenna, *Inorg. Chem.*, 2017, **56**, 9535–9546.
27 M. S. Khalaf, M. P. Coles and P. B. Hitchcock, *Dalton Trans.*, 2008, 4288–4295.
28 Y. J. Tsai, W. Lo and Q. Zhao, *Polyhedron*, 2015, **97**, 39–46.
29 S. Schmidt, S. Schulz, D. Bläser, R. Boese and M. Bolte, *Organometallics*, 2010, **29**, 6097–6103.
30 J. Lewiński, M. Dranka, I. Kraszewska, W. Sliwiński and I. Justyniak, *Chem. Commun.*, 2005, 4935–4937.
31 Z. Wróbel, I. Justyniak, I. Dranka and J. Lewiński, *Dalton Trans.*, 2016, **45**, 7240–7243.
32 M. A. Bhide, J. A. Manzi, C. E. Knapp and C. J. Carmalt, *Molecules*, 2021, **26**, 3165.
33 J. Barker, D. R. Aris, N. C. Blacker, W. Errington, P. R. Phillips and M. G. H. Wallbridge, *J. Organomet. Chem.*, 1999, **586**, 138–144.
34 K. Korona, M. Terlecki, I. Justyniak, M. Magott, J. Żukrowski, A. Kornowicz, D. Pinkowicz, A. Kubas and J. Lewiński, *Chem. – Eur. J.*, 2022, **28**, e202200620.
35 K. Korona, A. Kornowicz, I. Justyniak, M. Terlecki, A. Błachowski and J. Lewiński, *Dalton Trans.*, 2022, **51**, 16557–16564.
36 R. Neufeld and D. Stalke, *Chem. Sci.*, 2015, **6**, 3354–3364.
37 A. Kreyenschmidt, S. Bachmann, T. Niklas and D. Stalke, *ChemistrySelect*, 2017, **2**, 6957–6960.
38 S. J. Birch, S. R. Boss, S. C. Cole, M. P. Coles, R. Haigh, P. B. Hitchcock and A. E. H. Wheatley, *Dalton Trans.*, 2004, 3568–3574.
39 K. L. Orchard, A. J. P. White, M. S. P. Shaffer and C. K. Williams, *Organometallics*, 2009, **28**, 5828–5832.
40 J. Lewiński, M. Dranka, W. Bury, W. Śliwiński, I. Justyniak and J. Lipkowski, *J. Am. Chem. Soc.*, 2007, **129**, 3096–3098.
41 *CrysAlis PRO*, Agilent Technologies Ltd, Yarnton, Oxfordshire, England.
42 Z. Otwinowski and W. Minor, in *Methods in Enzymology*, 1997, vol. 276, pp. 307–326.
43 G. M. Sheldrick, *Acta Crystallogr., Sect. A: Found. Crystallogr.*, 2008, **64**, 112–122.